Cross-Links of Quadruplex Structures from Human Telomeric DNA by Dinuclear Platinum Complexes Show the Flexibility of Both Structures†

Isabelle Ourliac-Garnier,‡ Miguel-Angel Elizondo-Riojas,§ Sophie Redon,‡,|| Nicholas P. Farrell,⊥ and Sophie Bombard*,‡

Laboratoire de Chimie et Biochimie Pharmacologiques et Toxicologiques, UMR8601, Université René Descartes, 45 rue des Saints-Pères, 75270 Paris Cedex 06, France, Centro Universitario Contra el Cáncer, Hospital Universitario "Dr. José Eleuterio González", Universidad Autónoma de Nuevo León, Monterrey, N.L., Mexico, and Department of Chemistry, Virginia Commonwealth University, Richmond, Virginia 23284-2006

Received January 25, 2005; Revised Manuscript Received April 26, 2005

ABSTRACT: The folding of $AG_3(T_2AG_3)_3$ was investigated in the presence of Na^+ or K^+ ions, by using the dinuclear platinum complexes $[\{trans\text{-}PtCl(NH_3)_2\}_2H_2N(CH_2)_nNH_2]Cl_2$ ($n = 2$ or 6). $AG_3(T_2AG_3)_3$ has been previously found to adopt two different quadruplex structures: the antiparallel one in a solution containing Na^+ and the parallel one in a K^+-containing crystal. The two structures are strikingly distinct and are not expected to form the same platinum cross-links. Therefore, characterization of the cross-links formed with platinum complexes in solution allowed the predominant conformation(s) to be identified. The bases coordinating the platinum atoms were identified by chemical and 3′-exonuclease digestions. The observed cross-links showed that the parallel structure exists in solution whatever the cation and confirmed the existence of the antiparallel structure in the presence of both cations as previously reported from cross-linking experiments of $AG_3(T_2AG_3)_3$ by mononuclear platinum complexes. Furthermore, the major platinum cross-links were unexpectedly formed between two guanines belonging to the same G-quartet. Their formation was rationalized using molecular dynamics simulations in implicit solvent of the two quadruplex structures. It was shown that they were flexible, allowing some guanines to leave reversibly the top G-quartet and thus rendering their N_7 atom accessible to platinum complexes. Our results also suggest that the human telomere sequence could be a target for such platinum complexes.

Quadruplex structures are highly stable DNA or RNA structures formed on G-rich sequences (*1*). G-rich regions appear in several locations in the human genome, including telomeres at the ends of linear chromosomes (*2*), centromeres, fragile X syndrome repeats (*3*), and promoters of some genes (*4*). In vitro, such sequences have been shown to fold in quadruplex structures (*5*). The biological existence of quadruplexes has been demonstrated in vivo in the macronuclei of protozoans using a specific antibody generated against quadruplexes (*6*). Furthermore, there is a growing body of evidence which shows that they may have specific functional roles in vivo (*7*, *8*). In particular, quadruplex structures play a role in gene regulation of the c-myc promoter (*9*) and as inhibitors of the telomerase, an enzyme which provides cancerous cell immortality by adding guanine repeats at the ends of telomeres (*10*). The human quadruplexes of telomeric sequences have therefore received attention in the context of telomerase inhibition as a potential anticancer therapy using specific small molecules that are able to stabilize quadruplexes (*11*). Identification of the different foldings of quadruplexes in solution would help in the design of specific potent ligands.

Quadruplexes result from the stacking of planar G-quartets, the guanines being associated by Hoogsteen-type hydrogen bonds involving their N_7 atoms (Figure 1). Four consecutive repeats of guanines in the DNA sequence are required for the formation of an intramolecular quadruplex structure. The Na^+ and K^+ cations appear to stabilize quadruplexes by interacting with the electron-rich carbonyl oxygens of the eight guanines of two adjacent quartets (*12*, *13*). The human telomeric sequence contains repeats of TTAGGG ending in a single strand with overhangs of 100−200 bases at the end of the double strand (*14*). The single strand can fold in different quadruplex structures in vitro. $AG_3(T_2AG_3)_3$ has been found to adopt two different structures: the antiparallel structure (*15*) identified in a solution containing Na^+ and the parallel structure reported from an X-ray structure of a K^+-containing crystal (*16*) (Figure 1). The two structures differ by their strand orientation, the glycosidic conformations of guanines and their TTA loop orientations: the latter are located at each side of the quadruplex in the antiparallel structure and positioned alongside the grooves in the parallel structure. It was first thought that the parallel and the antiparallel folding of $AG_3(T_2AG_3)_3$ were due to the nature of the monovalent cation. Indeed, previous circular dichroism

† This work has been supported by L'Association pour la Recherche contre le Cancer (9799 3482) and COST (Action D20/003/01).

* To whom correspondence should be addressed. Phone: 33 1 42 86 22 56. Fax: 33 1 42 86 83 87. E-mail: sophie.bombard@univ-paris5.fr.

‡ Université René Descartes.

§ Universidad Autónoma de Nuevo León.

|| Current address: Swiss Institute for Experimental Cancer Research, 155 Chemin des Boveresses, 1066 Epalinges, Switzerland.

⊥ Virginia Commonwealth University.

10.1021/bi050144w CCC: $30.25
Published on Web 07/14/2005

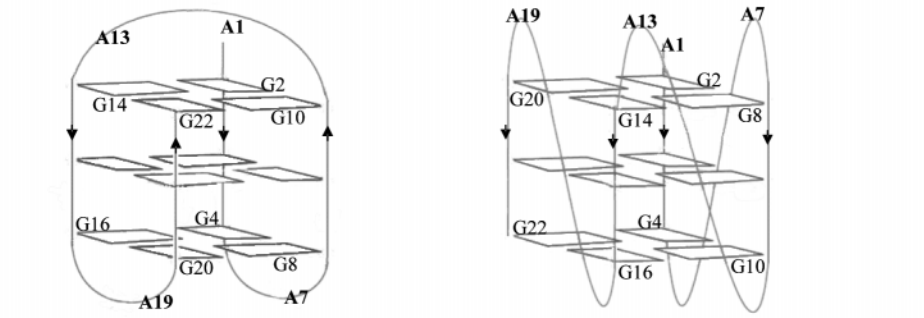

Anti-parallel structure **Parallel structure**

$A_1G_2G_3G_4T_5T_6A_7G_8G_9G_{10}T_{11}T_{12}A_{13}G_{14}G_{15}G_{16}T_{17}T_{18}A_{19}G_{20}G_{21}G_{22}$

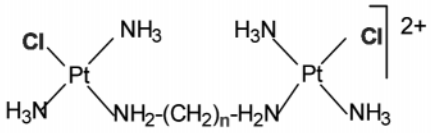

1.1/t,t n=2 or n=6

Trans-bisPt complexes

FIGURE 1: Schematic representation of the antiparallel structure of $AG_3(T_2AG_3)_3$, the parallel structure of $AG_3(T_2AG_3)_3$, and the dinuclear platinum complexes *trans*-bisPt(2) and *trans*-bisPt(6).

studies on the quadruplex structure of $AG_3(T_2AG_3)_3$ suggested that the antiparallel structure existed in the presence of Na^+ ions and that the presence of K^+ modified the conformation of the loops (*17*). Furthermore, multiple conformations of the human telomeric quadruplexes sequences have also been reported from UV spectrometry (*18*). Moreover, two recent studies have shown that the folding of $AG_3(T_2AG_3)_3$ does not depend only on the nature of the cation. We have recently shown that the antiparallel structure is not exclusively formed in the presence of Na^+ but also exists in K^+ solution (*19*). These results were obtained from studies of the platinum cross-linking of $AG_3(T_2AG_3)_3$ by the mononuclear platinum complexes *cis*- and *trans*-$[Pt(NH_3)_2(H_2O)_2]^{2+}$ in the presence of Na^+ or K^+. The platinum binding sites are N_7 atoms of guanines, provided that they are not involved in hydrogen bonds in the G-quartets and N_1 and N_7 atoms of adenines (*20*). In the quadruplex structures, two purines can be cross-linked by difunctional platinum complexes only if they are moving closer to each other thanks to the folding. Nevertheless, the parallel and antiparallel structures cannot form the same cross-links because of the different positions of the purines in the G-quartets and loops (Figure 1). Therefore, the mononuclear platinum complexes were able to cross-link the antiparallel structure of $AG_3(T_2AG_3)_3$, for which some N_7-N_7 distances were smaller than 4.5 Å, but not the parallel structure. Therefore, it was impossible to assert the presence of the latter in solution. Whether the parallel structure exists in a meaningful fraction of the species in solution thus remains to be demonstrated. Furthermore, recent single-FRET[1] measurements have shown that two stable folded conformations of the quadruplex structure of $AG_3(T_2AG_3)_3$ coexist in both Na^+- and K^+-containing solutions and that the two structures are in equilibrium (*21*). The authors cannot distinguish between the two structures by FRET, but they hypothesized that these corresponded to parallel and antiparallel quadruplex foldings.

Thanks to platinum complexes, our aim was to demonstrate the meaningful existence of the parallel structure in solution. For this study, we have chosen the dinuclear platinum complexes $[\{trans\text{-}PtCl(NH_3)_2\}_2H_2N(CH_2)_nNH_2]Cl_2$ ($n = 2$ or 6), subsequently named *trans*-bisPt(2) and *trans*-bisPt(6), respectively (Figure 1), for which two platinum coordination units are linked by a flexible diamine linker and the Pt−Pt distances are appropriate for cross-linking the parallel structure. These compounds have been designed in the search for novel classes of platinum antitumor compounds. They exhibit activity in tumor cells resistant to the mononuclear antitumor drug cisplatin (*22*). In contrast to the mononuclear platinum complexes for which the two purines are bound to the same platinum atom and the major sites of platination are two adjacent purines (*23*), the DNA cross-linking by the dinuclear platinum complexes is achieved by two independent monofunctional platinum sites. This leads to the formation not only of intrastrand G−G cross-links but also of long-range interstrand cross-links in duplex DNA where the sites of platination may be separated by up to four base pairs (*24*). Therefore, *trans*-bisPt complexes should be able to cross-link two purines in the proximity of the parallel structure that could not be cross-linked by the mononuclear platinum complexes. $AG_3(T_2AG_3)_3$ was platinated by *trans*-bisPt(2) and *trans*-bisPt(6) complexes in either Na^+- or K^+-containing solution. The platinum cross-links, identified by chemical and enzymatic digestions and using N_7-deazapurines, which are no longer platination sites, clearly demon-

[1] Abbreviations: FRET, fluorescence resonance energy transfer; DMS, dimethyl sulfate; *trans*-bisPt(6), $[\{trans\text{-}PtCl(NH_3)_2\}_2H_2N(CH_2)_6NH_2]Cl_2$; *trans*-bisPt(2), $[\{trans\text{-}PtCl(NH_3)_2\}_2H_2N(CH_2)_2NH_2]Cl_2$.

strate that the parallel quadruplex structure exists in both K^+ and Na^+ solution together with the antiparallel structure. They also identify some guanines that were unexpectedly accessible to platinum complexes. Molecular dynamics simulations show that these guanines can leave reversibly the G-quartets of the two structures, thus rendering their N_7 atom accessible to platinum complexes.

EXPERIMENTAL PROCEDURES

Chemicals. $AG_3(T_2AG_3)_3$, its derivatives containing one N_7-deazaguanine or one N_7-deazaadenine, and its complementary sequence, $(C_3TA_2)C_3T$, were synthesized and purified by Eurogentec, desalted on a Sephadex G25 column, and stored at −20 °C in a 1 mM aqueous solution. [{*trans*-$PtCl(NH_3)_2\}_2H_2N(CH_2)_nNH_2$] ($n = 2$ and 6) compounds [*trans*-bisPt(2) and *trans*-bisPt(6), respectively] were prepared as described previously (*25*). $[Pt(NH_3)_3(H_2O)]^{2+}$ was prepared from $[Pt(NH_3)_3(H_2O)](NO_3)_2$ as previously described (*26*).

5′-End Labeling of Oligonucleotides. The oligonucleotides were 5′-end-labeled using polynucleotide kinase (Pharmacia Biotech) and [γ-^{32}P]ATP (Pharmacia Biotech). The reaction products were purified via 20% denaturing gel electrophoresis and desalted on a Sephadex G25 column.

Platination of $AG_3(T_2AG_3)_3$ and $AG_3(T_2AG_3)_3$ Containing a N_7-Deazapurine in the Presence of Na^+ or K^+. The 5′-end-radiolabeled $AG_3(T_2AG_3)_3$ was mixed with 100 μM non-radiolabeled material in 50 mM $NaClO_4$ or $KClO_4$ for 5 min at 90 °C and allowed to reach room temperature in 2 h to induce the formation of quadruplex structure. It was then incubated with 120 μM *trans*-bisPt(2) or *trans*-bisPt(6) or 300 μM $[Pt(NH_3)_3(H_2O)]^{2+}$. The reactions were carried out for 16 h at 37 °C for the two *trans*-bisPt complexes and for 2 h for $[Pt(NH_3)_3(H_2O)]^{2+}$. For some experiments, 10 mM $NaClO_4$ at 43 °C and 100 mM $KClO_4$ at 37 °C were used. The number of platinum complexes bound per oligonucleotide was checked by mass spectrometry. The platination sites were determined from DMS/piperidine cleavage and 3′-exonuclease digestion (see below). The platinum cross-links were deduced (i) from the percent of protection from the DMS/piperidine cleavage at each guanine position (as the amount of protection corresponds to the amount of guanines platinated at this position; two guanines involved in the same cross-link are protected to the same extent) and (ii) using N_7-deazaguanines that are no longer platination sites. If one guanine was replaced with a N_7-deazaguanine, the formation of the cross-link(s) involving the guanine would be prevented.

trans-BisPt(2) and *trans*-bisPt(6) were able to cross-link two adjacent guanines on a double-stranded DNA (*27*, *28*). We have compared the platinated products of $AG_3(T_2AG_3)_3$ previously structured either in quadruplexes or in the double strand. The 5′-end-radiolabeled $AG_3(T_2AG_3)_3$ was mixed with 100 μM non-radiolabeled material and the complementary strand $(C_3TA_2)C_3T$ (100 μM) in 50 mM $NaClO_4$ or $KClO_4$ for 5 min at 90 °C and allowed to reach room temperature in 5 h to induce the formation of the double strand. The number of platinum complexes bound per oligonucleotide was checked by mass spectrometry. DMS/piperidine cleavage and enzymatic digestion of the platinated products (band 4 from Figure 2) showed that all the guanines were partially platinated, indicating that band 4 is a mixture of oligonucleotides cross-linked on different G positions.

For mass spectrometry analysis, the platination reactions were carried out with 2 nmol of non-radiolabeled $AG_3(T_2AG_3)_3$.

Platinated oligonucleotides were separated by 20% polyacrylamide denaturing gel electrophoresis and located either by autoradiography when mixed with radiolabeled oligonucleotides or by UV shadowing in the absence of labeling. They migrated differently according to their masses and charges.

Identification of Free Guanines by DMS/Piperidine Cleavage. The 5′-end-radiolabeled $AG_3(T_2AG_3)_3$ or $AG_3(T_2AG_3)_3$ containing a N_7-deazaguanine was mixed with 100 μM non-radiolabeled material in 50 mM $NaClO_4$, $KClO_4$, or water for 5 min at 90 °C and allowed to reach room temperature in 2 h to induce the formation of quadruplex structure. It was then incubated with 100 μM, 300 μM, 1 mM, or 10 mM DMS for 2 h at 37 °C. After precipitation, the oligonucleotides were treated with 50 μL of 1 M piperidine at 90 °C for 20 min. After evaporation of the piperidine, the oligonucleotides were migrated via 20% denaturing gel electrophoresis.

Mass Spectrometry. The major platinated products were analyzed by matrix-assisted laser desorption ionization (MALDI) mass spectrometry with a linear time-of-flight (TOF) analyzer matrix using 2,4,6-trihydroxyacetophenone.

Nondenaturing Gel Electrophoresis. Nondenaturing gel electrophoresis of $AG_3(T_2AG_3)_3$ and its N_7-deazapurine derivatives was performed as previously described (*29*) with 12% polyacrylamide gels (29:1 acrylamide:bisacrylamide ratio) containing tris(hydroxymethyl)aminomethane-borate [0.088 M Tris-borate (pH 8.3)] and EDTA (0.002 M) in 50 mM KCl at 4 °C. Gel migration lasted 18 h at 140 V.

Identification and Quantification of the Platinum Binding Sites by DMS. After their separation by gel electrophoresis, the different products of the platination reaction were eluted from the gel and ethanol precipitated. The platinated products were treated with DMS/piperidine (probe of the free N_7) under Maxam−Gilbert sequencing conditions. The oligonucleotides were dissolved in 20 μL of water and incubated with 1 μL of DMS for 1 min at 37 °C. After precipitation, the oligonucleotides were incubated with 50 μL of 1 M piperidine at 90 °C for 20 min. After evaporation of the piperidine, the oligonucleotides were deplatinated with 0.2 M NaCN overnight and migrated via 20% denaturing gel electrophoresis (*29*). The amount of cleavage at each guanine was quantified using a Dynamics Molecular Phosphorimager with Imagequant for data processing. As the N_7-platinated guanines are no longer reactive with dimethyl sulfate (DMS), the platinated sites can be deduced from the absence or lower intensity of the spots corresponding to the cleavable guanosines. For each guanine, we compared, under exactly identical conditions, the percentage of DMS/piperidine cleavage for the nonplatinated and platinated oligonucleotides, and for each guanine, we deduced the percentage of protection of cleavage. The percentage of protection of cleavage was calculated for each guanine as {[% of cleavage of nonplatinated $AG_3(T_2AG_3)_3$] − [% of cleavage of platinated $AG_3(T_2AG_3)_3$]}/[% of cleavage of nonplatinated $AG_3(T_2AG_3)_3$] (*29*). The platinated and nonplatinated oligonucleotides were not structured during the DMS treatment because

they resulted from a denaturing gel electrophoresis, and the DMS/piperidine treatment was carried out in water to prevent the folding of the quadruplex structure. Moreover, if the quadruplex structure had been formed, the guanines from the G-quartets would have been protected from DMS/piperidine cleavage, which was not the case. The maximal experimental error was evaluated to be 15%, limiting the analysis to major adducts.

Identification of the Platinum Binding Sites by 3′-Exonuclease Digestion. We used 3′-exonuclease digestion to identify all the adenine and guanine platination sites, including the minor ones, that could not be detected by the DMS/piperidine treatment. This enzyme has already been used to identify the platination sites of quadruplexes cross-linked by mononuclear platinum complexes: its digestion is stopped by platinum monoadducts or chelates. Nevertheless, with an increase in the concentration, this enzyme can bypass the first platinated base encountered, that is, the 3′-base of the platinum cross-link (*19*). Therefore, the two platinum sites of a cross-link can be identified by enzymatic digestion using an increasing enzyme concentration. The platinated products, isolated from gel electrophoresis, were incubated in 10 mM Tris-HCl (pH 8.0) in the presence of 2 mM $MgCl_2$ and 0.5 mg/mL tRNA with the 3′-exonuclease phosphodiesterase I from *Crotalus adamanteus* venom (UBS) at 0.008 and 0.04 unit/μL for 30 min at 37 °C. The partial digestion of nonplatinated oligonucleotide was carried out at a concentration of 0.001 unit/μL. The digested fragments were purified on a 20% denaturing gel. The migration of the fragments depends on the presence of platinum adducts; therefore, each of them has been eluted from the gel, precipitated, and deplatinated with 2 M NaCN for 18 h at 37 °C. After precipitation in ethanol, the deplatinated fragments migrated on 20% denaturing gel. Their migrations were compared to those of the fragments obtained by partial digestion of the starting oligonucleotide. From their migration, we can determine their length and consequently identify the platinated base at which the 3′-exonuclease stopped its digestion.

Molecular Dynamics Simulations in Implicit Solvent of the Antiparallel and Parallel Quadruplex Structure of $AG_3(T_2AG_3)_3$. MD simulations in implicit solvent were carried out with the SANDER module of AMBER 7.0 (*30*). The atomic coordinates (PDB entries 143D and 1KF1) were used to build the starting antiparallel (*15*) and parallel (*16*) structures, respectively.

The structures were first minimized in implicit solvent without any restraint, with 500 steps of the steepest descent and 1500 steps of the conjugate gradient minimizers. For the unrestrained MD simulations in implicit solvent, we applied the published protocol (*31*), with the parm98.dat force field (*32*), a 20 Å cutoff, a time step of 1 fs, and nrespa = 4. Each structure was then heated from 0 to 300 K over the course of 40 ps with a harmonic restraint force of 5 kcal mol^{-1} $Å^{-2}$ to keep the atoms at their initial positions during the heating. Then, three equilibration steps of 40, 40, and 20 ps were used with the harmonic constant reduced to 1.0, 0.1, and 0.0 kcal mol^{-1} $Å^{-2}$, respectively. After equilibration, a production step of 10 ns without restraint was run. A structure was recorded after each picosecond leading, by the end of the simulation, to 10 000 snapshots. Panels A and B of Figure 9 were generated using VMD (*33*).

Determination of Distances between the Purine Nitrogens as Potential Cross-Linking Sites from the Digestion Data. The N−N distances (in angstroms) of the antiparallel (*15*) and parallel structures (*16*) were measured, using the CARNAL module of AMBER 7.0, in the 10 000 structures isolated during the 10 ns molecular dynamics simulations.

Determination of Accessibility of the Purine Nitrogens of Both Quadruplex Structures. The accessible area on the van der Waals surfaces of the N_7 atoms for each guanine and the N_1 and N_7 atoms for each adenine was measured for the 10 000 structures isolated during the 10 ns molecular dynamics simulations reported on the antiparallel and parallel structures. It was calculated with a spherical probe with a 4.9 Å van der Waals radius corresponding to the hydratation form of a platinum atom (*34*). The accessible nucleophilic part of the N_7 and N_1 atoms was defined as the surface of a solid angle of 30° from the bisector line between the N_7 atom and the center of the pentacycle or the bisector between the N_1 atom and the center of the hexacycle.

Molecular Dynamics Simulations in Implicit Solvent of the Dinuclear Platinum Complexes trans-BisPt(2) and trans-BisPt(6). The atomic charges for the two dinuclear platinum complexes $[\{trans\text{-}PtCl(NH_3)_2\}_2H_2N(CH_2)_nNH_2]^{2+}$ (n = 2 and 6) were derived from a density functional theory calculation employing the B3LYP hybrid functional implemented in Gaussian 03 (*35*); the LANL2DZ pseudopotential/pseudoorbital basis set was used for Pt and the all-electron 3-21G* basis set for the other atoms. The atomic charges were determined from fits to the electrostatic potentials using the Merz−Kollman routine (*36*); charges of chemically identical atoms were averaged.

The MD simulations in implicit solvent were carried out as described for $AG_3(T_2AG_3)_3$ except that the complexes $[\{trans\text{-}PtCl(NH_3)_2\}_2H_2N(CH_2)_nNH_2]^{2+}$ (n = 2 and 6) were used and that the parm98 force field (*32*) was complemented with parameters describing the platinum coordination sphere (*37*−*39*). A structure was recorded after each picosecond leading, by the end of the simulation, to 10 000 snapshots. The Pt−Pt distances (in angstroms) were measured, using the CARNAL module of AMBER 7.0, for the 10 000 structures isolated during the 10 ns molecular dynamics simulations.

Construction and Molecular Dynamics Simulations of the Antiparallel and Parallel Structures Cross-Linked by trans-BisPt(2) and trans-BisPt(6), Respectively. The atomic charges for the two dinuclear platinum complexes $[\{trans\text{-}Pt(NH_3)_2(Guo)\}_2H_2N(CH_2)_nNH_2]^{4+}$ (n = 2 and 6) were derived from a density functional theory calculation on the 9-methylguanine derivative $[\{trans\text{-}Pt(NH_3)_2(9\text{-}Me\text{-}Guo)\}_2H_2N(CH_2)_nNH_2]^{4+}$, employing the B3LYP hybrid functional implemented in Gaussian 03 (*35*); the LANL2DZ pseudopotential/pseudoorbital basis set was used for Pt and the all-electron 3-21G* basis set for the other atoms. The atomic charges were determined from fits to the electrostatic potentials using the Merz−Kollman routine (*36*); charges of chemically identical atoms were averaged.

The cross-linked antiparallel and parallel structures were derived from starting structures of PDB entries 143D and 1KF1, respectively, by on-screen manipulations using VMD (*33*) combined with simulating annealing and energy minimization techniques using AMBER 7.0 (*30*).

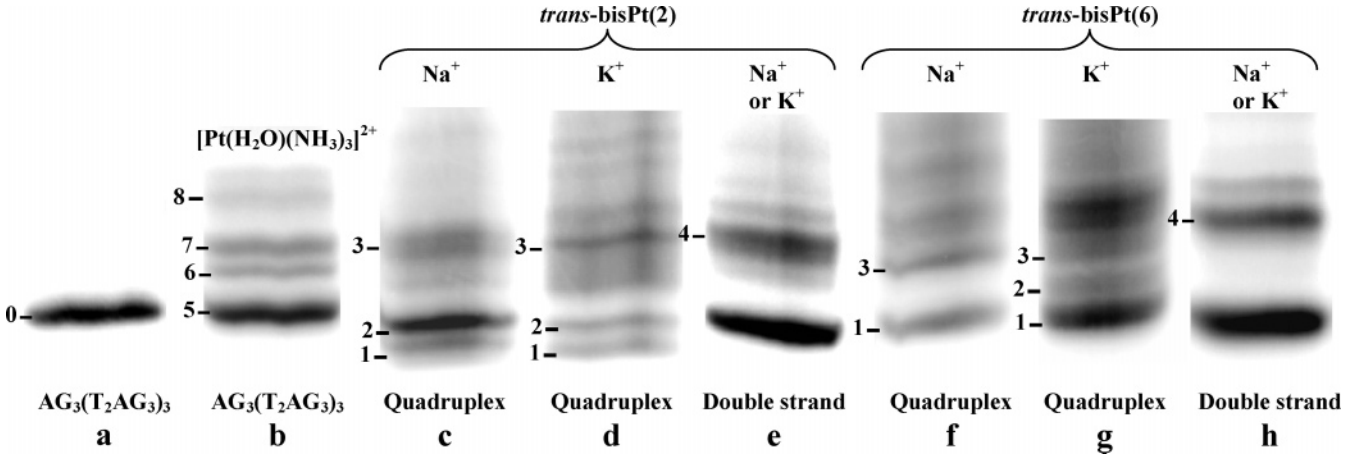

FIGURE 2: Denaturing gel electrophoresis (20% acrylamide) of $AG_3(T_2AG_3)_3$ (lane a) and the products of platination of $AG_3(T_2AG_3)_3$ by $[Pt(H_2O)NH_3)_3]^{2+}$ (lane b), by *trans*-bisPt(2) in Na^+ solution (lane c), by *trans*-bisPt(2) in K^+ solution (lane d), by *trans*-bisPt(2) on the double strand of $AG_3(T_2AG_3)_3$ (lane e), by *trans*-bisPt(6) in Na^+ solution (lane f), by *trans*-bisPt(6) in K^+ solution (lane g), and by *trans*-bisPt(6) on the double strand of $AG_3(T_2AG_3)_3$ (lane h).

Table 1: MALDI-TOF Mass Spectrometry of the Products of $AG_3(T_2AG_3)$ Platinated by *trans*-BisPt(2) and *trans*-BisPt(6) in Na^+ or K^+ Solution, Separated by Gel Electrophoresis

platinum complex	platinated product[a]	mass found	mass calcd for $AG_3(T_2AG_3)$
none	**0**	7043.9	7046.59 with 0 complexes bound
trans-bisPt(2)	**1**	7563.3	7564.59 with 1 complex bound
	2	7559	7564.59 with 1 complex bound
	3	7573	7564.59 with 1 complex bound
		8079	8082.59 with 2 complexes bound
	4	7501.8	7496.59 with 1 complex bound ($-4NH_3$)[b]
trans-bisPt(6)	**1**	7625	7620.59 with 1 complex bound
	2	7613	7620.59 with 1 complex bound
	3	7621	7620.59 with 1 complex bound
		8194	8194.59 with 2 complexes bound
	4	7558.89	7552.59 with 1 complex bound ($-4NH_3$)[b]
$[Pt(H_2O)(NH_3)_3]^{2+}$	**5**	7044.3	7046.59 with 0 complexes bound
	6 and **7**	7281.3	7275.59 with 1 complex bound ($-NH_3$)[b]
	8	7473.2	7470.59 with 2 complexes bound ($-4NH_3$)[b]

[a] The number of the platinated product is the one used for the bands isolated from the gel of Figure 2. [b] In mass spectrometry, it is common for platinum complexes to lose one (or more) NH_3 during the analysis (*57*, *58*).

The MD simulations in implicit solvent were carried out as described for $AG_3(T_2AG_3)_3$ except that the parm98 force field (*32*) was extended to account for platinum−guanine coordination, as described by Herman et al. (*40*) and Elizondo-Riojas et al. (*41*). The four improper torsion angle terms used to parametrize the bending of the $Pt-N_7$ bonds out of the guanine planes (*40*) were reduced according to the method of Chval and Šíp (*42*) to account for guanine puckering. A structure was recorded after each picosecond leading, by the end of the simulation, to 10 000 structures. Finally, the average structures of the cross-linked antiparallel and parallel structures were obtained from the 10 000 snapshots. These structures were fully minimized without any restraint with the GB model until a norm of the energy gradient of ≤ 0.1 was achieved. Panels A and B of Figure 10 were generated using VMD (*33*).

RESULTS

Determination of the Type of Adduct after Platination of $AG_3(T_2AG_3)_3$ Folded in the Presence of Na^+ or K^+ Cations, by Dinuclear Platinum Complexes trans-BisPt(2) and trans-BisPt(6). $AG_3(T_2AG_3)_3$ was first folded in the presence of 50 mM Na^+ or K^+. It was then reacted with *trans*-bisPt(2) or *trans*-bisPt(6) in a 1:1.2 ratio. Products of the platination reaction were separated on denaturing gels (Figure 2, lanes c, d, f, and g). The products of platination were analyzed by MALDI-TOF mass spectrometry (Table 1). Bands 1 and 2 (each being 35−50% of the starting material) contained one *trans*-bisPt bound per oligonucleotide, whereas the other bands (including band 3) consisted of a mixture of oligonucleotides bearing one or two *trans*-bisPt complexes. They migrated as a function of their charge (additional 4+ charge per *trans*-bisPt), mass (one or two *trans*-bisPt complexes), and the possible presence of a cross-link between remote purines in the sequence. It has been previously shown that a cisplatin chelate of two adjacent purines or a monoadduct bound to one purine has a retarded migration, whereas a cisplatin chelate of two remote purines accelerates the migration of platinated oligonucleotides (*19*, *29*). The two *trans*-bisPt complexes can form three types of adducts: a monoadduct, a bifunctional cross-link between two adjacent purines (i.e., 1,2 or 1,3 GG cross-links) as already shown for the double-stranded DNA (*27*, *28*), or a bifunctional cross-link between two purines remote in the primary sequence but close enough in the three-dimensional quadruplex structure.

We have examined the nature of the adducts obtained from the platination of $AG_3(T_2AG_3)_3$ by *trans*-bisPt by comparing

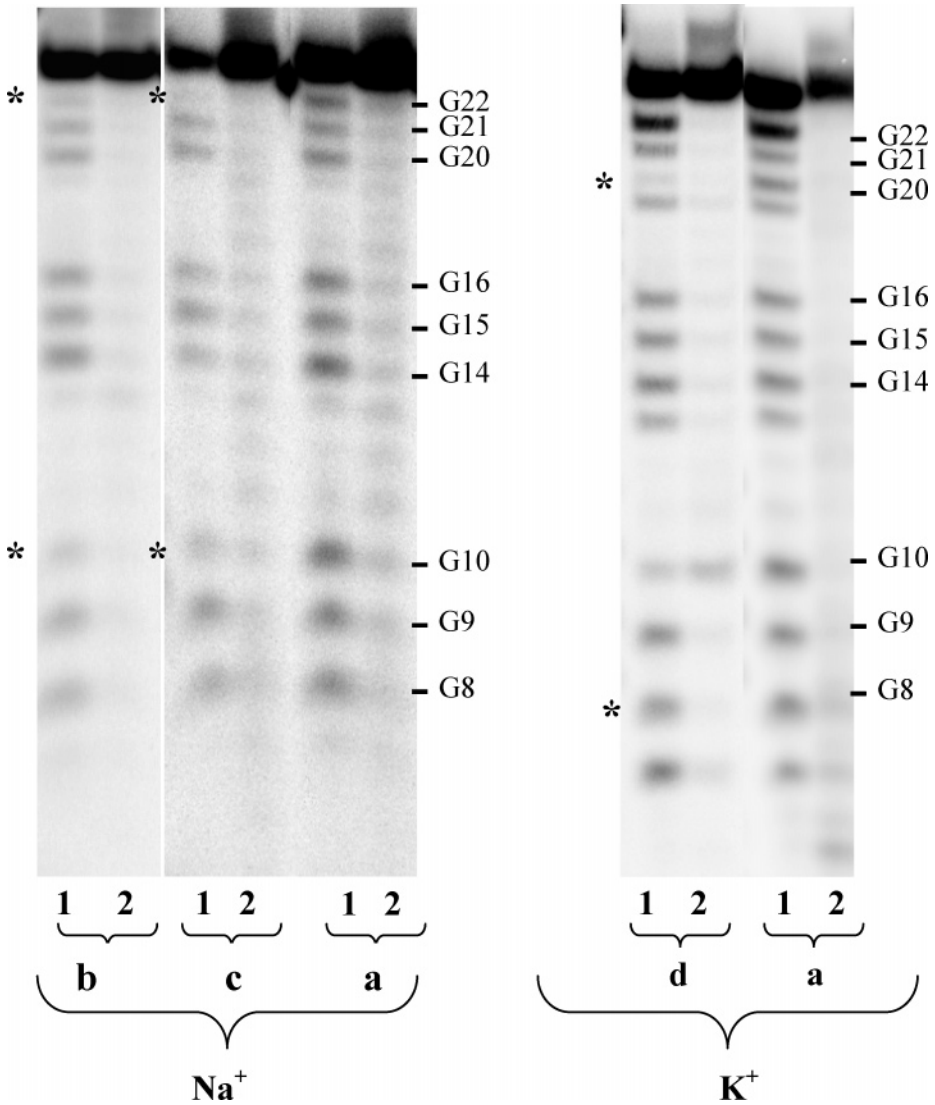

FIGURE 3: Denaturing gel electrophoresis of the DMS/piperidine cleavage of $AG_3(T_2AG_3)_3$ (a), of the platinated product of band 1 from reaction of $AG_3(T_2AG_3)_3$ with *trans*-bisPt(2) in Na^+ (b), of the platinated product of band 1 from reaction of $AG_3(T_2AG_3)_3$ with *trans*-bisPt(6) in Na^+ (c), or in K^+ (d). Lane 1 shows DMS/piperidine treatment and lane 2 piperidine treatment. The percentage of protection of cleavage was calculated for each guanine as {[% of cleavage of nonplatinated $AG_3(T_2AG_3)_3$] − [% of cleavage of platinated $AG_3(T_2AG_3)_3$]}/[% of cleavage of nonplatinated $AG_3(T_2AG_3)_3$].

their migration to those of two known platinum adducts: cross-links of *trans*-bisPt between two adjacent guanines in duplex DNA (lanes e and h in Figure 2) and monoadducts of the monofunctional platinum complex $[Pt(H_2O)(NH_3)_3]^{2+}$ (lane b in Figure 2). In the first control experiment, $AG_3(T_2AG_3)_3$ was annealed with its complementary strand to form the double strand. It has already been shown that the presence of the complementary strand of $AG_3(T_2AG_3)_3$ favored the double strand over its quadruplex structure at the salt concentration used for the platination reactions (*43*). The double strand was then platinated by *trans*-bisPt(2) and *trans*-bisPt(6) in a 1:1.2 ratio to obtain 1,2 or 1,3 cross-links of *trans*-bisPt between two guanines (*27*, *28*). One major platination product was obtained (band 4, lanes e and h). MALDI-TOF mass spectrometry (Table 1) indicated that one *trans*-bisPt was bound per oligonucleotide. All 12 guanines were partially platinated (see Experimental Procedures). These results indicated that band 4 was a mixture of $AG_3(T_2AG_3)_3$ cross-linked by *trans*-bisPt at different guanine positions. Products from band 4 migrated much more slowly than products from bands 1 and 2, suggesting that the oligonucleotides from bands 1 and 2 were not cross-linked in a similar manner by *trans*-bisPt. In another control experiment, $AG_3(T_2AG_3)_3$ was reacted with 2 equiv of the monofunctional $[Pt(H_2O)(NH_3)_3]^{2+}$ complex and was then migrated on a denaturing gel (Figure 2, lane b). Because *trans*-bisPt complexes consist of two $[Pt(NH_3)_3]^{2+}$ entities linked by a short alkyl chain, the migration of a monoadduct of *trans*-bisPt(2) and *trans*-bisPt(6) should be similar to that of $AG_3(T_2AG_3)_3$ bearing two $[Pt(NH_3)_3]^{2+}$ moieties. The platination reaction by $[Pt(H_2O)(NH_3)_3]^{2+}$ led to three platinated products: bands 6 and 7 contained one $[Pt(NH_3)_3]^{2+}$ bound per oligonucleotide, whereas the platinated oligonucleotides isolated from band 8 contained two $[Pt(NH_3)_3]^{2+}$ moieties bound per oligonucleotide. Products from band 8 migrated more slowly than products from bands 1 and 2, suggesting that products from bands 1 and 2 were not monoadducts of *trans*-bisPt complexes.

In conclusion, the faster gel migration of the platinated products from bands 1 and 2 compared to the migration of the products cross-linked between two adjacent purines (band 4) and of the products bearing two $[Pt(NH_3)_3]^{2+}$ moieties

(band 8) indicated that the platinated products from bands 1 and 2 were cross-linked between two remote purines in the sequence. This result was relevant to the cross-linking of a quadruplex structure of $AG_3(T_2AG_3)_3$. This was confirmed by the fact that, if the platination reaction had occurred on the unfolded form of $AG_3(T_2AG_3)_3$, all the N_7 atoms would have been accessible and susceptible to platination; therefore, only cross-links between two adjacent guanines or monoadducts would have been formed, and the platinated products would have migrated as in band 4 or 8.

The platination reactions were also performed in the presence of 10 mM Na^+ at 43 °C or 100 mM K^+ at 37 °C which were the conditions used to analyze the folding of $AG_3(T_2AG_3)_3$ by single-FRET measurement (*21*). The same platination profiles as shown in Figure 2 were obtained.

Identification of Platinum Binding Sites and Identification of Platinum Cross-Links. Platinum cross-links were determined only for products from bands 1 and 2 that indicated the trapping of a quadruplex structure. Their platination sites were identified. They were the same whatever the salt concentration (10−100 mM) and the temperature of the platination reaction (37−43 °C). The cross-links were determined from the quantification of platinated bases and were confirmed by using N_7-deazaguanines which are no longer platinum binding sites. They were then attributed to the parallel or antiparallel structures considering the position of the platinum binding sites within the two structures and the distance between the two platinum atoms.

Platination of $AG_3(T_2AG_3)_3$ by trans-BisPt(2) in Na^+ or K^+ Solution. The identification of the platinum binding sites of the cross-links from band 1 (lanes c and d of Figure 2) was first performed using DMS, a probe of free N_7-guanine. As the N_7-platinated guanines are no longer reactive toward dimethyl sulfate (DMS), the platinated sites could be deduced from the absence or reduction of the extent of cleavage at these positions (*29*). G10 and G22 of the products from band 1 were protected from DMS/piperidine cleavage with 60% efficiency (Figure 3), indicating that 60% of $AG_3(T_2AG_3)_3$ was platinated on G10 and/or G22. Two bases involved in the same platinum cross-link were protected with the same efficiency; therefore, our results suggested that the G10−G22 cross-link was the major cross-link of *trans*-bisPt(2). Whether this cross-link was compatible with the parallel or antiparallel structure (Figure 1) will be discussed below.

The formation of a G10−G22 cross-link has been further confirmed by using a modified $AG_3(T_2AG_3)_3$ sequence in which G10 or G22 was replaced with N_7-deaza-G, which are no longer platination sites. Therefore, the replacement of a guanine with N_7-deaza-G prevents the formation of the platinum cross-link involving this guanine. These oligonucleotides were still able to fold in quadruplex structure as checked by their accelerated migration in nondenaturing gel electrophoresis (Figure 4) and the protection of their guanines to DMS/piperidine cleavage in Na^+ or K^+ solution (Figure 1 of the Supporting Information). This result indicated that the replacement of the N_7 with C_7 had no influence on the formation of the quadruplex, even if it impedes the formation of one of the eight hydrogen bonds from an external G-quartet. This result was in accordance with experiments showing that the replacement of one guanine of a G-quartet with inosine (deletion of the NH_2 group of the guanine involved in one hydrogen bond of the G-quartet) did not prevent the formation of a quadruplex structure (*44*, *45*). When $AG_3(T_2AG_3)_3$ containing either N_7-deaza-G10 or N_7-deaza-G22 was incubated with *trans*-bisPt(2) in Na^+ or K^+ solution (lanes b, c, e, and f of Figure 5), a weaker or no band 1 was detected, indicating that the G10−G22 cross-link was the major platinum cross-link of band 1. The absence of the G10−G22 cross-link was not due to the unfolding of the quadruplex structure because the remaining bands 1 and 2 were still formed. Otherwise, all the platinated products would have migrated like bands 4 and 8 (Figure 2).

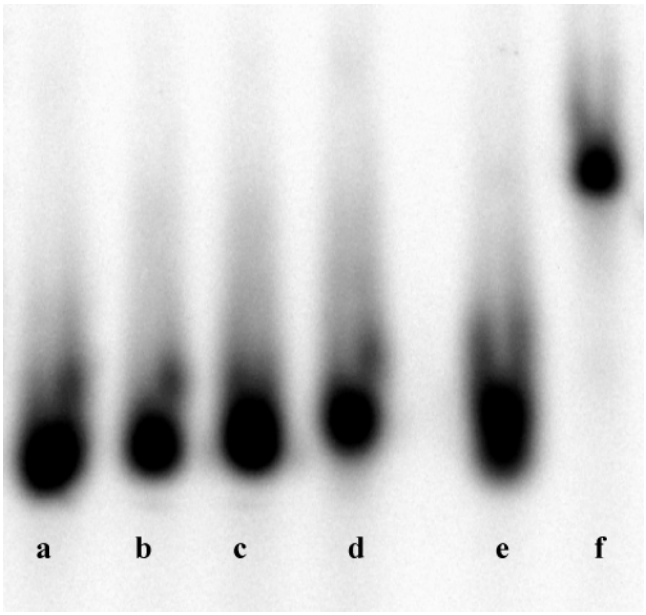

FIGURE 4: Nondenaturing gel electrophoresis (12% acrylamide) of $AG_3(T_2AG_3)_3$ containing N_7-deaza-G22 (lane a), $AG_3(T_2AG_3)_3$ containing N_7-deaza-G20 (lane b), $AG_3(T_2AG_3)_3$ containing N_7-deaza-G10 (lane c), $AG_3(T_2AG_3)_3$ containing N_7-deaza-G8 (lane d), $AG_3(T_2AG_3)_3$ (lane e), and $AG_3(T_2AG_3)_3$ containing N_7-deaza-G15−G21 (lane f). The latter cannot fold anymore.

An exonuclease digestion was necessary for the identification of minor platination sites of the products from band 1. As the oligonucleotides were 5′-labeled, the 3′-exonuclease was used. It stopped its digestion at each platinated site (*19*). One digested fragment was obtained for each stop of digestion. The digested fragments were purified on gel (Figure 6A). Their migration depends on their size, but as it was influenced by the presence of a platinum complex, the fragments were deplatinated. They migrated again on an electrophoresis gel to determine their size from which the platination site was deduced (Figure 6B). It is noteworthy that mononucleotide A1 (band VI of Figure 6A) and dinucleotide A1G2 (band V of Figure 6A) bearing the *trans*-bisPt migrated more slowly than $AG_3(T_2AG_3)_3$. This was due to the presence of the 4+ charge of the platinum complex on a very short oligonucleotide: indeed, it has been shown that the major contribution to the electrophoretic mobility of very short oligonucleotides (fewer than four nucleotides) is their charge and not their length (*46*). This phenomenon has already been observed for short platinated RNA oligonucleotides and for digested platinum adducts of cisplatin on $AG_3(T_2AG_3)_3$ (*19*, *47*). The 3′-exonuclease digestion of the oligonucleotides from band 1 gave six platinated fragments (Figure 6A) identifying, after their deplatination, the following platination sites: A1, G2, G10, A19, G20, and

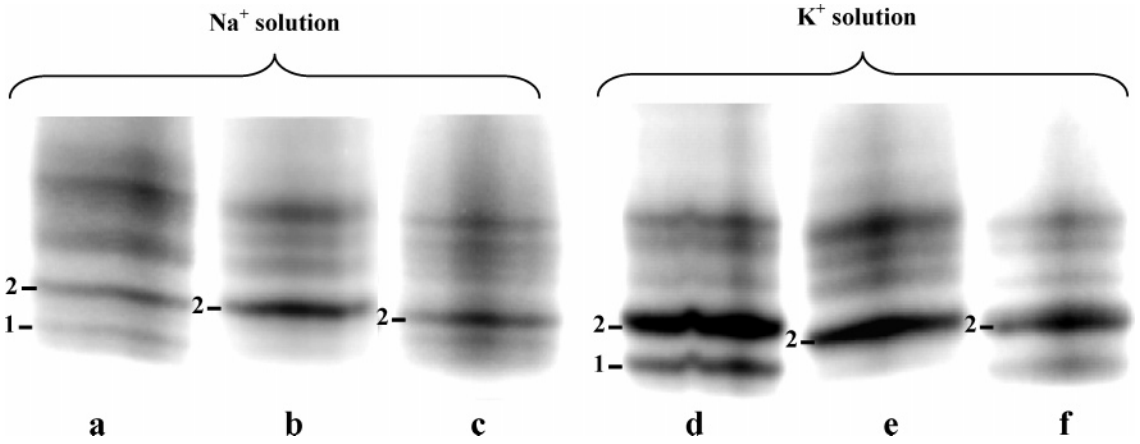

FIGURE 5: Denaturing gel electrophoresis (20% acrylamide) of the platination products by *trans*-bisPt(2), in Na^+ solution of $AG_3(T_2AG_3)_3$ (lane a), of $AG_3(T_2AG_3)_3$ containing N_7-deaza-G22 (lane b), and of $AG_3(T_2AG_3)_3$ containing N_7-deaza-G10 (lane c) or in K^+ solution of $AG_3(T_2AG_3)_3$ (lane d), of $AG_3(T_2AG_3)_3$ containing N_7-deaza-G22 (lane e), and of $AG_3(T_2AG_3)_3$ containing N_7-deaza-G10 (lane f).

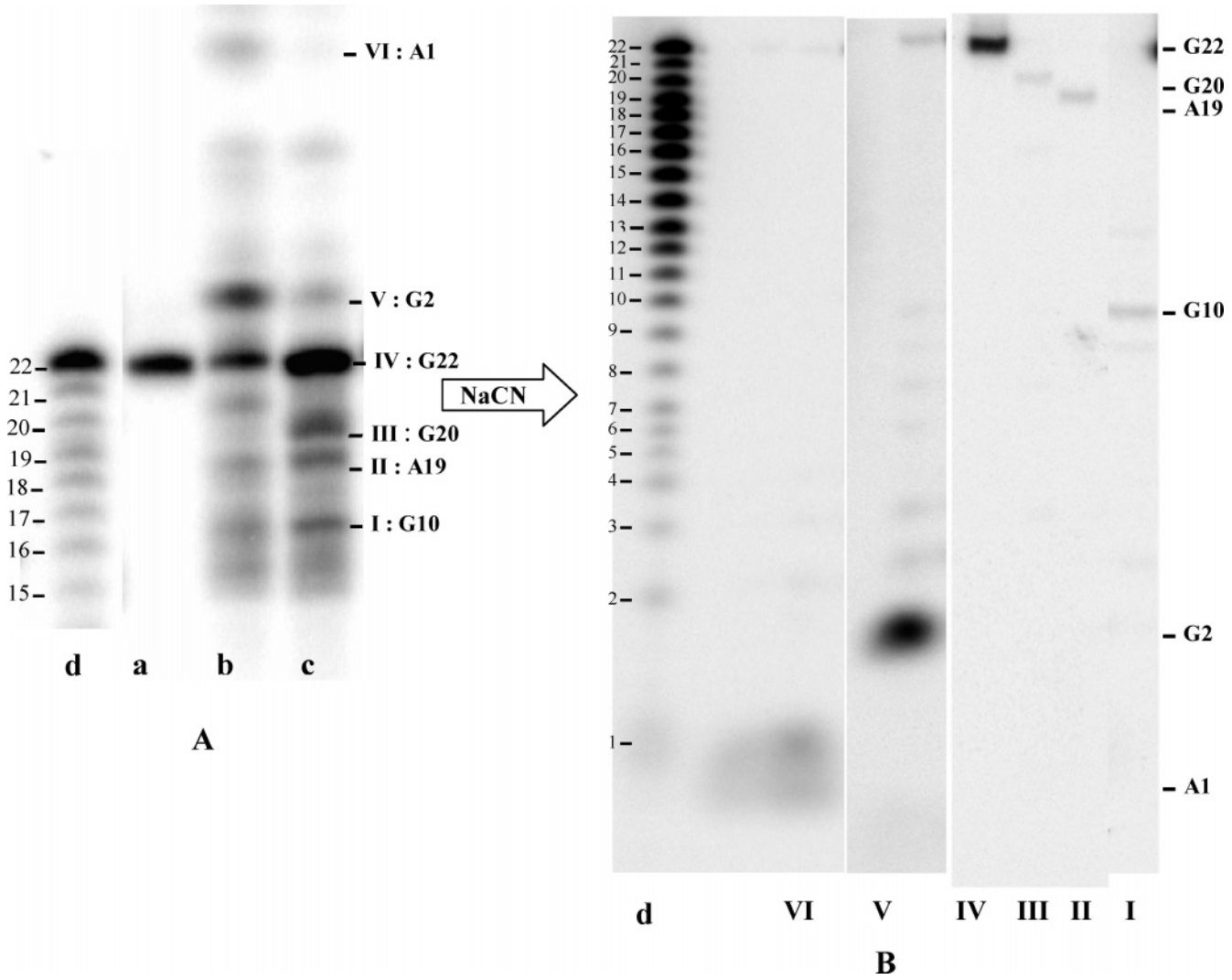

FIGURE 6: (A) Denaturing gel electrophoresis of the 3′-exonuclease digestion of the platinated products obtained from reaction of $AG_3(T_2AG_3)_3$ with *trans*-bisPt(2), in Na^+ or K^+ solution (band 1, lanes c and d of Figure 2). The digestion reaction was conducted with different enzyme dilutions: lane a, no enzyme; lane b, 0.04 unit of enzyme/μL; and lane c, 0.008 unit of enzyme/μL. Lane d corresponds to the partial digestion of nonplatinated $AG_3(T_2AG_3)_3$, with an enzyme dilution of 0.001 unit/μL; it gives the reference scale for the migration of the platinated digested fragments. (B) Denaturing gel electrophoresis of the fragments of digestion (in Roman numerals) after deplatination by NaCN. The numbered purines correspond to the digestion arrests.

G22 (Figure 6B). It has been concluded that the following cross-links were formed: G10−G22 as the major one in accordance with the DMS/piperidine treatment and two minor A1−A19 and G2−G20 cross-links that were deduced (and/or G2−A19 and A1−G20). The A1−G2 and A19−G20 cross-links were not considered possible cross-links in

band 1 because they would have migrated like band 4 that contains cross-links between adjacent purines.

The platinated products from band **2** (lanes c and d of Figure 2) were treated with DMS/piperidine and exonuclease digestion. G2 and G14 were protected from the DMS/piperidine cleavage with 40% efficiency, suggesting that the G2−G14 cross-link was the major cross-link. This result was confirmed by the 3′-exonuclease digestion of the oligonucleotides from band 2 which resulted in two digested products (Figure 7A, and Figure 2 of the Supporting Information) identifying G2 and G14 as platination sites and the G2−G14 cross-link as the major cross-link of band 2.

Platination of $AG_3(T_2AG_3)_3$ by trans-BisPt(6) in Na^+ Solution. The platinated products from band 1 (lane f of Figure 2) were treated with DMS/piperidine and 3′-exonuclease digestion. G10 and G22 were protected from DMS/piperidine cleavage with 60% efficiency, indicating that 60% of the oligonucleotides were cross-linked between G10 and G22 (Figure 3). The major G10−G22 cross-link was confirmed by using $AG_3(T_2AG_3)_3$ containing either N_7-deaza-G10 or N_7-deaza-G22. No G10−G22 cross-link was formed when either of these two modified oligonucleotides was platinated with *trans*-bisPt(6): no band 1 or a weaker one was detected. The 3′-exonuclease yielded approximately six products of digestion, identifying G2, G8, G10, G14, G20, and G22 as platination sites (Figure 7B, and Figure 4 of the Supporting Information). It has been concluded that the following cross-links were formed: G10−G22 as the major one in accordance with the DMS/piperidine treatment and G8−G20 and G2−G14 as the minor ones. The attribution of these minor cross-links was confirmed by the platination of $AG_3(T_2AG_3)_3$, whose G8, G14, and G20 were replaced with their corresponding N_7-deaza-G. All these modified oligonucleotides were able to fold in quadruplex structure as shown by their accelerated migration, like the nonmodified $AG_3(T_2AG_3)_3$ on nondenaturing gel electrophoresis (Figure 4) and the protection of the guanines from cleavage by DMS/piperidine (Figure 1 of the Supporting Information). Band 1 was formed wherever the N_7-deaza-G was placed in $AG_3(T_2AG_3)_3$, and the 3′-exonuclease digestion of the products contained in band 1 still revealed the major presence of a G10−G22 cross-link. However, when $AG_3(T_2AG_3)_3$ was modified at N_7-deaza-G14, G2 was not detected as a platination site of the oligonucleotides from band 1; therefore, the G2−G14 cross-link was not detected. When $AG_3(T_2AG_3)_3$ was modified at N_7-deaza-G8 or N_7-deaza-G20, G20 or G8, respectively, was no longer a platinum site of the oligonucleotides from band 1 and the G8−G20 cross-link was not detected.

Platination of $AG_3(T_2AG_3)_3$ by trans-BisPt(6) in K^+ Solution. G8 and G20 of the platinated products from band **1** (lane g of Figure 2) were protected from DMS/piperidine cleavage with 60% efficiency, indicating that the major platination product was the G8−G20 cross-link (Figure 3). Furthermore, in the presence of $AG_3(T_2AG_3)_3$ containing N_7-deaza-G8 or N_7-deaza-G20, the G8−G20 platinum cross-link was not detected (no band 1 or weaker one). The 3′-exonuclease digestion of band 1 resulted in six fragments (Figure 7C, and Figure 4 of the Supporting Information), identifying A1, G2, G8, G10, A19, and G20 as platination sites. They were involved in the three following platinum cross-links: G8−G20, the major one in accordance with

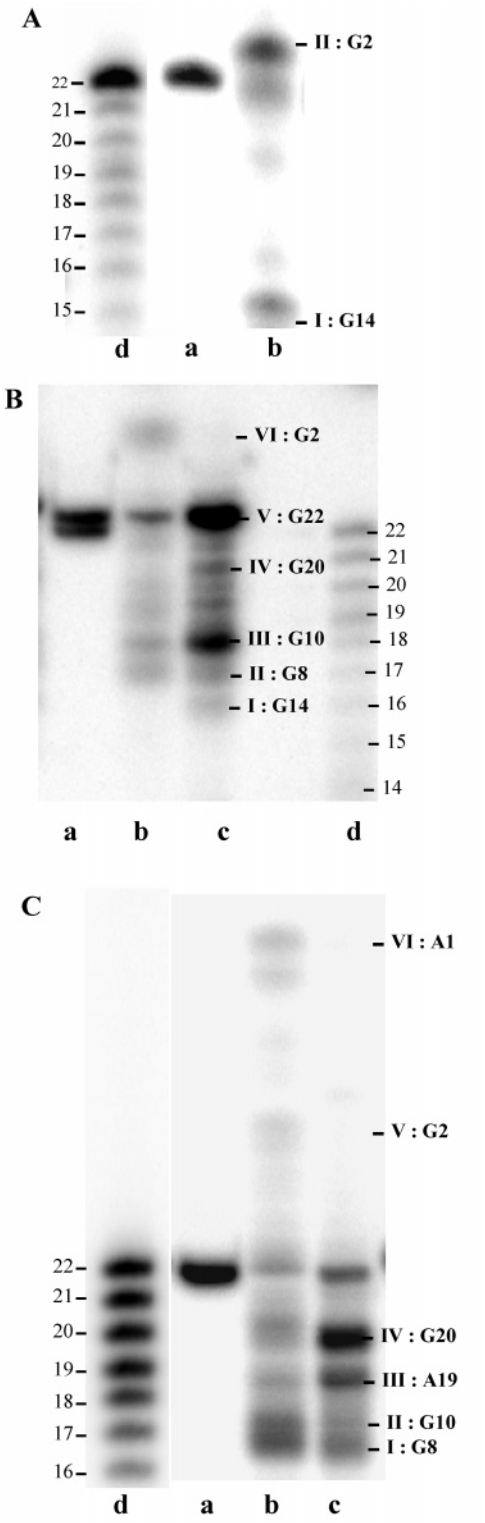

FIGURE 7: Denaturing gel electrophoresis of the fragments (in Roman numerals) from the 3′-exonuclease digestion of the platinated products of $AG_3(T_2AG_3)_3$ from reaction with *trans*-bisPt(2), in Na^+ and K^+ solution (A) (band 2, lanes c and d of Figure 2), and with *trans*-bisPt(6), in Na^+ (B) (band 1, lane f of Figure 2) and in K^+ (C) (band 1, lane g of Figure 2). The digestion reaction was conducted with different enzyme dilutions: lane a, no enzyme; lane b, 0.04 unit of enzyme/μL; lane c, 0.008 unit of enzyme/μL; and lane d, 0.001 unit of enzyme/μL. The numbered purines correspond to the digestion arrests. They were determined from the migration of the corresponding fragments after deplatination by NaCN (see Figures 2−4 of the Supporting Information). The partial digestion of $AG_3(T_2AG_3)_3$ (lane d) gives the reference scale for the migration of the platinated digested fragments.

Table 2: Platinum Cross-Links of $AG_3(T_2AG_3)_3$ Folded in Na^+ or K^+ Solution by *trans*-BisPt(2) and *trans*-BisPt(6) Formed on the Parallel and Antiparallel Quadruplex Structures[a]

trans-bisPt(2) Pt−Pt distances of 5.3−7.6 Å		*trans*-bisPt(6) Pt−Pt distances of 7.8−12.4 Å			
Na^+	K^+	Na^+	K^+	structure	N_7-N_7 distance (Å)
G10*−*G22[1]	***G10*−*G22***[1]	***G10*−*G22***[1]		**antiparallel *top***	6.2−9.3
G2*−*G14[2]	***G2*−*G14***[2]	*G2*−*G14*[1]		**antiparallel *top***	7.2−8.7
		G8−*G20*[1]	**G8−*G20***[1]	**parallel *top***	10.5−12
G2−*G20*[1]	G2−*G20*[1]		G2−*G20*[2]	parallel *top*	6.5−8.5
			G2−*G10*[1]	antiparallel *top*	6.2−9.8
A1−A19[1]	*A1*−A19[1]		*A1*−A19,[1] A−A,[2] and A−G[2]	parallel	>7

[a] The major cross-links are indicated in bold. The bases in italics are the ones in which N_7 or N_1 atoms have been found to be accessible to platinum complexes in the 10 000 structures isolated from molecular dynamics in implicit solvent without any constraint; the underlined bases are the most accessible purines. The N_7-N_7 distances between two purines of the antiparallel and parallel structures were measured on the 10 000 isolated structures from molecular dynamics simulations. The superscript numerals indicate that these cross-links were found in bands 1 and 2, respectively, of Figure 2.

DMS/piperidine treatment, G2−G10, and A1−A19. A1−G2 and G10−A19 cross-links were not taken into account because the A1−G2 cross-link would have migrated like band 4 that contains cross-links between adjacent purines. Besides, the G10−A19 cross-link is not compatible with either of the two structures. No clear inhibition of cleavage by DMS/piperidine treatment was observed for the oligonucleotides from band **2** (lane g of Figure 2), indicating either that the platination sites were the adenines or that each comigrating product represents less than 15% of the total amount of oligonucleotides. The 3′-exonuclease digestion of the platinated products from band 2 resulted in nine fragments identifying the following platination sites: A1, G2, A7, A13, G14, G16, A19, G20, and G22. As these cross-links were obtained only in the presence of K^+, we hypothesized that they were only formed on the parallel structure, including many A−A and A−G cross-links. However, because of the great number of platination sites, it was difficult to determine the nature of each cross-link.

Attribution of Platinum Cross-Links to a Structure and Evidence of the Presence of the Parallel Structure in Solution. Therefore, the platination reactions of $AG_3(T_2AG_3)_3$ by the two *trans*-bisPt complexes in Na^+ or K^+ solutions led therefore to the formation of six cross-links that indicated the trapping of a quadruplex structure in solution because they involved remote but not adjacent guanines in the sequence. Considering the position of the purines within the two structures and the distances between the two platinum atoms of *trans*-bisPt complexes, we could deduce which quadruplex structure had been cross-linked. G10−G22, G2−G14, and G8−G20 cross-links could be interpreted on both the parallel and antiparallel structures (Figure 1), whereas the G2−G10 cross-link could only be formed on the antiparallel structure and G2−G20 and A1−A19 cross-links only on the parallel structure (Table 2 and Figure 8). Therefore, the cross-linking of the parallel structure highlighted the meaningful existence of the parallel structure in solution. The attribution of the G10−G22, G2−G14, and G8−G20 cross-links to one of the two structures needed further investigation. To this aim, we have checked the accessibility of guanines of both structures to the monofunctional platinum complex $[Pt(H_2O)(NH_3)_3]^{2+}$ and to dimethyl sulfate, and we also used molecular dynamic simulations.

Identification of the First Platination Sites: Comparison between the Reactivity of Guanines toward $[Pt(H_2O)(NH_3)_3]^{2+}$ and Dimethyl Sulfate. The surprising point of these results was that some guanines were platinated. Since their N_7 atom was expected to be involved in hydrogen bonds of G-quartets, they should not have been platination sites any longer. To determine the first platination sites, $AG_3(T_2AG_3)_3$ was platinated, in the presence of Na^+ or K^+, by the monofunctional $[Pt(H_2O)(NH_3)_3]^{2+}$, and the products of monoplatination (band 7, lane b in Figure 2) were analyzed using 3′-exonuclease digestion. G8, G10, A13, G14, G20, and G22 were found to be platinated, indicating that they were the purines most accessible to platinum complexes. In a parallel experiment, DMS was used to detect the accessibility of the different guanines. DMS methylates the N_7 atoms of guanines and is widely used as an indicator of quadruplex structures because it can detect which guanines are involved in a G-quartet (*9*, *48*). $AG_3(T_2AG_3)_3$ was treated with DMS, followed by piperidine cleavage, under the same incubation conditions as $[Pt(H_2O)(NH_3)_3]^{2+}$, of water or Na^+ or K^+ solution. When $AG_3(T_2AG_3)_3$ was folded in the presence of K^+, all the guanines were protected from the cleavage by DMS/piperidine treatment, while in the presence of Na^+, all the guanines were protected from DMS, except G10, G14, and G22 which appeared to be less protected: they were cleaved in a small amount compared to $AG_3(T_2AG_3)_3$ in water (Figure 5 of the Supporting Information). These results were in accordance with the first platination sites identified by $[Pt(H_2O)(NH_3)_3]^{2+}$ but showed that DMS was less sensitive to the detection of the slipping of the guanines than platinum complexes. It was then necessary to understand why the N_7 atoms of some guanines located in a

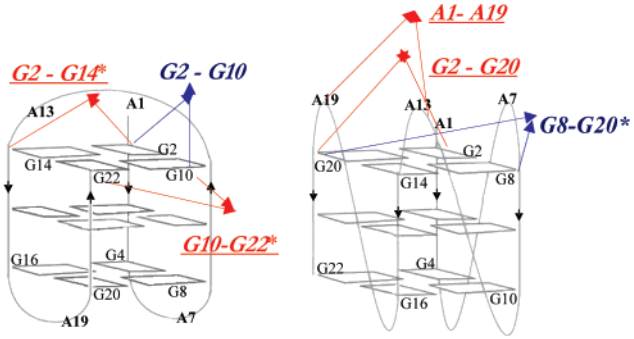

FIGURE 8: Schematic representation of the various platinum cross-links formed upon reaction of the two quadruplex structures of $AG_3(T_2AG_3)_3$ with both *trans*-bisPt(2) and *trans*-bisPt(6) (red) and with only *trans*-bisPt(6) (blue). The major ones are denoted with asterisks.

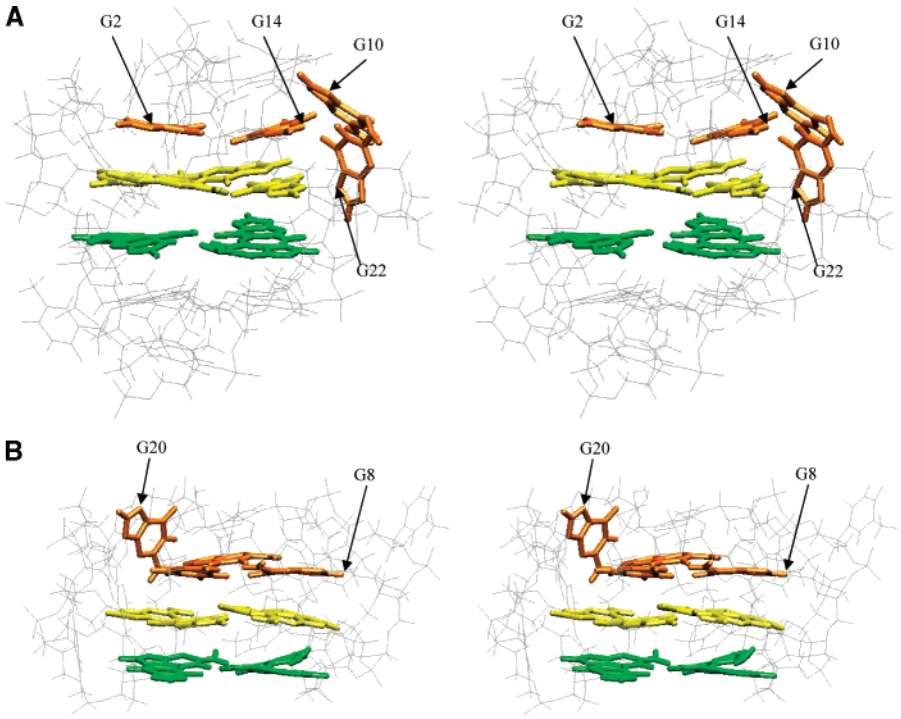

FIGURE 9: (A) Stereoview of a snapshot conformation of the antiparallel structure of $AG_3(T_2AG_3)_3$ taken at 8202 ps from the 10 ns length MD simulation in implicit solvent. (B) Stereoview of a snapshot conformation of the parallel structure of $AG_3(T_2AG_3)_3$ taken at 1233 ps from the 10 ns length MD simulation in implicit solvent.

G-quartet were able to be platinated and cross-linked by the *trans*-bisPt complexes.

Molecular Dynamics Simulations in Implicit Solvent of Antiparallel and Parallel Quadruplex Structures of $AG_3(T_2AG_3)_3$: Attribution of G10−G22, G2−G14, and G8−G20 Cross-Links to One Structure. Unconstrained molecular dynamics simulations in implicit solvent were run on the antiparallel and parallel structures (Figure 1) for 10 ns; 10 000 structures from these dynamics simulations were isolated. The surface accessible to platinum has been analyzed for each nucleophilic atom (N_7 of guanines and N_7 and N_1 of adenines) of each of the 10 000 snapshots and was calculated with a spherical probe with a van der Waals radius of 4.9 Å corresponding to the hydratation form of a platinum atom (*34*). The data were recorded as a function of time (Figure 6 of the Supporting Information). The analysis of the plots allowed us to distinguish the N_7 atoms of the following purines which were accessible to the platinum complex. For the antiparallel structure, G2, G10, G14, and G22 are the four guanines belonging to the top G-quartet, G14 and G22 being the most accessible ones along with three of the four adenines (A1, A7, and A13). These results were in accordance with the first platination sites of $AG_3(T_2AG_3)_3$ depicted with $[Pt(H_2O)(NH_3)_3]^{2+}$ (G10, A13, G14, and G22). Figure 9 is a representative snapshot of the antiparallel and parallel structures isolated from the dynamics simulations. They clearly show that the top G-quartet located at the top of the antiparallel structure, involving G2, G10, G14, and G22, is disrupted, allowing the N_7 atoms of the different guanines to be platinated and consequently to form the G10−G22, G2−G14, and G2−G10 cross-links. On the contrary, the bottom G-quartet was stable during molecular dynamics simulations, indicating that the G8−G20 platinum cross-link cannot be formed on the antiparallel structure, whereas on the parallel structure, G20 and A1 are found to be the most accessible purines by molecular dynamics (Figure 6 of the Supporting Information). G20 has also been found to be accessed by $[Pt(H_2O)(NH_3)_3]^{2+}$. G20 slipped out of the top G-quartet, whereas G2, G14, and G8 formed a guanine base triplet (Figure 9). The first platination process should occur on G20, allowing the subsequent formation of G8−G20 and G2−G20 cross-links. Together with the A1−A19 cross-link, the formation of these two platinum cross-links gave evidence of the existence of the parallel structure in solution.

Assuming that the cross-linking reaction depends on the distance of the second N_7 atom and on the distance of the second platinum atom, the N_7-N_7 distances were measured between the purines of the different cross-links. They were recorded between G10 and G22, G2 and G14, and G2 and G10 for the 10 000 structures of the antiparallel structure and between G8 and G20, G2 and G20, and A1 and A19 for the 10 000 structures of the parallel structure (Table 2). They were compared to the Pt−Pt distances of *trans*-bisPt-(2) and *trans*-bisPt(6) that were measured from dynamics molecular simulations in implicit water without any constraint (Table 2). They showed that all the N_7-N_7 distances of the G−G cross-links were compatible with the Pt−Pt distances of either the two *trans*-bisPt complexes (G10−G22, G2−G14, and G2−G20) or *trans*-bisPt(6) only (G2−G10 and G8−G20). Furthermore, the A1−A19 cross-link was formed only on the parallel structure for which the N−N distances were >7 Å. No A−A cross-link was formed on the antiparallel structure for which the distances were <4.5 Å, a distance too short for cross-linking by the *trans*-bisPt complexes.

To evaluate the stability of the two quadruplex structures cross-linked by *trans*-bisPt, we have constructed the G10−G22 cross-link of *trans*-bisPt(2) on the antiparallel structure and the G8−G20 cross-link of *trans*-bisPt(6) on the parallel

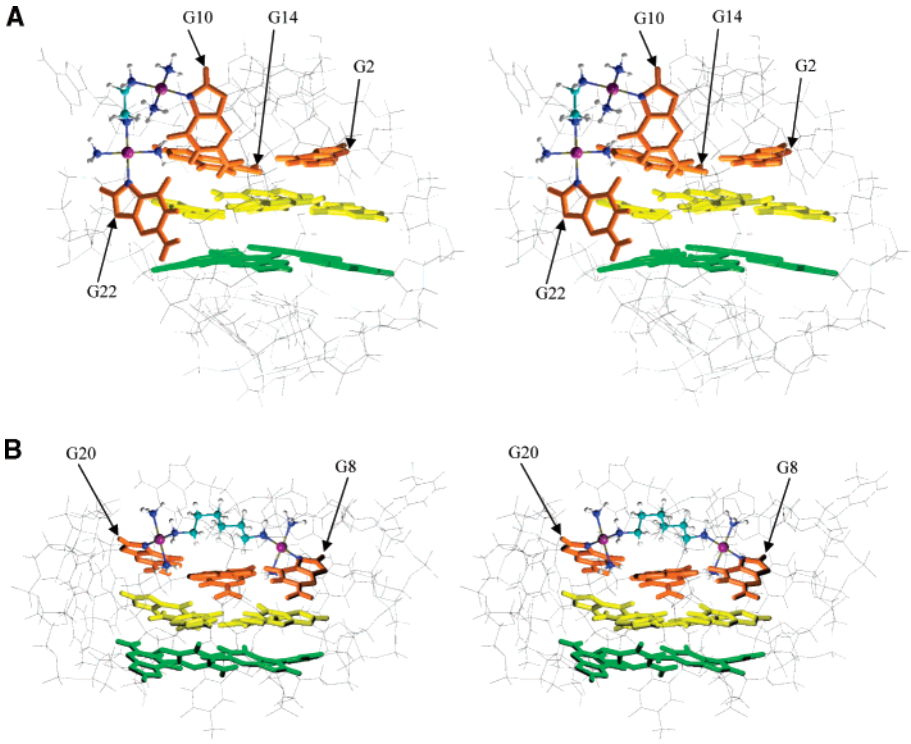

FIGURE 10: Stereoview of the average energy-minimized structures from 10 ns length MD simulations in implicit solvent of the antiparallel structure cross-linked by *trans*-bisPt(2) between G10 and G22 (A) and of the parallel structure cross-linked by *trans*-bisPt(6) between G8 and G20 (B).

structure and carried out unconstrained molecular dynamics simulations in implicit solvent for 10 ns on these platinated structures. Figure 10 clearly shows that the alkyl chain of the dinuclear platinum complexes is sufficiently long to cross-link two guanines without inducing a deformation or a destabilization of the overall quadruplex structures.

In summary, the cross-linking experiments of $AG_3(T_2AG_3)_3$ by the two *trans*-bisPt complexes in Na^+ or K^+ solutions indicate that the parallel and antiparallel structures actually coexist in solution containing either Na^+ or K^+. It is noteworthy that only the guanines belonging to the top G-quartet of the two structures were the major platination sites. These guanines have been shown, by molecular dynamics simulations, to slip out of the G-quartet, thus rendering their N_7 atom accessible to platinum complexes.

DISCUSSION

The aim of our work was to demonstrate the meaningful existence of the parallel structure of $AG_3(T_2AG_3)_3$ in solution. The folding of $AG_3(T_2AG_3)_3$, in the presence of Na^+ or K^+ ions, was investigated using the two dinuclear platinum complexes [{*trans*-$PtCl(NH_3)_2$}$_2$$H_2N(CH_2)_nNH_2$]$Cl_2$ ($n = 2$ and 6), *trans*-bisPt(2) and *trans*-bisPt(6). The parallel and antiparallel structures (Figure 1) cannot form the same cross-links because of the different positions of the purines in the G-quartets and loops. Therefore, characterization of the cross-links formed with platinum complexes in solution allowed the predominant conformation(s) to be identified. Three platinum cross-links have been identified on the parallel structure, and three others have been identified on the antiparallel structure whatever the nature of the cation in solution (Figure 8 and Table 2). These cross-links gave evidence that the parallel structure exists in solution in meaningful proportions. Moreover, they showed that the parallel structure is not exclusively formed in K^+ solution but that it also exists in Na^+ solution. They also confirmed the existence of the antiparallel structure in the presence of both cations as previously reported from cross-linking experiments of $AG_3(T_2AG_3)_3$ with the mononuclear platinum complexes *cis*- and *trans*-$[Pt(NH_3)_2(H_2O)_2](H_2O)_2$ (*19*). They are in agreement with the recent results of ^{125}I radioprobing data, published during the preparation of this paper, demonstrating the presence of the antiparallel and parallel conformations in solution in the presence of both K^+ and Na^+ (*49*).

These results lead to the conclusion that the antiparallel and parallel structures can correspond to the two stable conformations of $AG_3(T_2AG_3)_3$ which were previously demonstrated to be in equilibrium using single-molecule FRET dynamics studies (*21*) and/or correspond to the two foldings of $AG_3(T_2AG_3)_3$ observed by Raman and UV spectroscopy (*18*). Using *trans*-bisPt(6) and 50 mM cations, we showed that the parallel structure is mainly formed in the presence of K^+, whereas the antiparallel structure is mainly formed in the presence of Na^+. However, we were not able to change the proportion between the two structures significantly, using higher K^+ concentrations or lower Na^+ concentrations, as used in the single-molecule FRET experiments (*21*). As our platination reactions were performed at 100 μM, 2×10^6 times higher than in the single-molecule FRET experiment (50 pM), intermolecular interactions may modify the equilibrium. Furthermore, the coexistence of the parallel and antiparallel structures in solution is consistent with the finding that the two-repeat telomeric sequence $(TAG_3)_2T$ forms interconverting parallel and antiparallel G-quadruplexes in solution (*50*). However, a mechanism for

the structural transition from the antiparallel to the parallel quadruplex remains to be investigated.

It is noteworthy that most platinum cross-links involve two guanines despite the expected involvement of their N_7 atoms in hydrogen bonding. The unexpected reactivity of some guanines was interpreted by molecular dynamics simulations showing a disruption of hydrogen bonds, within the top G-quartet, followed by the rotation of the guanines out of the G-quartet. The existence of such conformations has already been observed for other quadruplex structures. A disruption of hydrogen bonds within an external G-quartet, analogous to the antiparallel structure of $AG_3(T_2AG_3)_3$ (Figure 10A), has been described for the quadruplex of $(G_4T_4G_4)_2$ in the presence of Ca^{2+} (*51*, *52*), and the G-triad observed on the parallel structure of $AG_3(T_2AG_3)_3$ (Figure 10B) has been proposed as a possible intermediate in the process of quadruplex folding (*53*).

The top G-quartet of the antiparallel structure can be completely disrupted, whereas the top G-quartet of the parallel structure can lose one guanine and subsequently form a G-triad. These results suggest that a transversal loop (identical to the $T_{11}T_{12}A_{13}$ sequence of the antiparallel structure) can disrupt the adjacent outer G-quartet, whereas a double lateral loop (identical to the $T_5T_6A_7$ and $T_{17}T_{18}A_{19}$ sequences of the antiparallel structure) or double reversal loops positioned alongside the grooves (on the parallel structure) cannot. It has been found that the stability of the human telomeric quadruplexes, checked by its melting temperature, was increased by 12 °C in the presence of K^+ compared to Na^+ (*54*). This difference has been previously attributed to the ionic radius and the free energies of hydration of the cation because full dehydration of the cation is required for coordination of O_6 (*55*). On the basis of the relative stability of the top G-quartet of the two structures, we may now suggest that the stability of a quadruplex structure might also depend on the stability of outer G-quartets which is correlated with the geometry of the adjacent loops. Moreover, from recent NMR structural analyses of two dimeric quadruplexes of $(TG_4T)_2$, it has been suggested that the stabilization contribution of the G-quartet core (through the syn/anti distribution of the guanines) is probably much larger than those of the loops (*56*). Our results do not confirm this hypothesis because they indicated that the top and bottom G-quartets of the antiparallel structure do not show the same stability despite their similar guanine arrangement (syn/syn/anti/anti).

Finally, our cross-linking experiments showed that platinum complexes are good tools for the trapping of quadruplex structures: as expected, the cross-links depend on the number of platinum atoms (mono- or dinuclear) and on the length of the alkyl chain linking the two platinum atoms of the dinuclear complexes. They could also be used in the detection of the transient free N_7 atoms of guanines, whereas DMS is less sensitive.

In conclusion, as the dinuclear platinum complexes can promote long-range cross-links, they are able to cross-link the two quadruplex structures of the human telomeric sequence $AG_3(T_2AG_3)_3$ whereas the mononuclear platinum complexes are able to cross-link the antiparallel structure only. The cross-linking experiments have also emphasized the flexibility of the two structures, because some guanines can reversibly leave the quartet plane, thus rendering their N_7 atom accessible to platinum complexes. From a biological point of view, these cross-links might lead to the inhibition of the telomerase.

ACKNOWLEDGMENT

We are indebted to Dr. J. C. Blais at Laboratoire de Chimie Organique Structurale, Université Pierre et Marie Curie, Paris, France, for mass spectrometry analyses. We thank Professor J. C. Chottard and Dr. J. Kozelka for helpful discussions.

SUPPORTING INFORMATION AVAILABLE

Denaturing gel electrophoresis results for various cleavages (Figures 1−5) and plots of the accessible areas of the van der Waals surfaces of the nitrogen atoms of the purines (Figure 6). This material is available free of charge via the Internet at http://pubs.acs.org.

REFERENCES

1. Neidle, S., and Parkinson, G. N. (2003) The structure of telomeric DNA, *Curr. Opin. Struct. Biol. 13*, 275−283.
2. Wright, W. E., Tesmer, V. M., Huffman, K. E., Levene, S. D., and Shay, J. W. (1997) Normal human chromosomes have long G-rich telomeric overhangs at one end, *Genes Dev. 11*, 2801−2809.
3. Usdin, K. (1998) NGG-triplet repeats form similar intrastrand structures: Implications for the triplet expansion diseases, *Nucleic Acids Res. 26*, 4078−4085.
4. Simonsson, T., Pecinka, P., and Kubista, M. (1998) DNA tetraplex formation in the control region of c-myc, *Nucleic Acids Res. 26*, 1167−1172.
5. Gilbert, D. E., and Feigon, J. (1999) Multistranded DNA structures, *Curr. Opin. Struct. Biol. 9*, 305−314.
6. Schaffitzel, C., Berger, I., Postberg, J., Hanes, J., Lipps, H. J., and Pluckthun, A. (2001) In vitro generated antibodies specific for telomeric guanine-quadruplex DNA react with *Stylonychia lemnae* macronuclei, *Proc. Natl. Acad. Sci. U.S.A. 98*, 8572−8577.
7. Neidle, S., and Read, M. A. (2000) G-Quadruplexes as therapeutic targets, *Biopolymers 56*, 195−208.
8. Arthanari, H., and Bolton, P. H. (2001) Functional and dysfunctional roles of quadruplex DNA in cells, *Chem. Biol. 8*, 221−230.
9. Siddiqui-Jain, A., Grand, C. L., Bearss, D. J., and Hurley, L. H. (2002) Direct evidence for a G-quadruplex in a promoter region and its targeting with a small molecule to repress c-MYC transcription, *Proc. Natl. Acad. Sci. U.S.A. 99*, 11593−11598.
10. Mergny, J. L., Riou, J. F., Mailliet, P., Teulade-Fichou, M. P., and Gilson, E. (2002) Natural and pharmacological regulation of telomerase, *Nucleic Acids Res. 30*, 839−865.
11. Rezler, E. M., Bearss, D. J., and Hurley, L. H. (2002) Telomeres and telomerases as drug targets, *Curr. Opin. Pharmacol. 2*, 415−423.
12. Hud, N. V., Schultze, P., Sklenar, V., and Feigon, J. (1999) Binding sites and dynamics of ammonium ions in a telomere repeat DNA quadruplex, *J. Mol. Biol. 285*, 233−243.
13. Phillips, K., Dauter, Z., Murchie, A. I., Lilley, D. M., and Luisi, B. (1997) The crystal structure of a parallel-stranded guanine tetraplex at 0.95 Å resolution, *J. Mol. Biol. 273*, 171−182.
14. Simonsson, T. (2001) G-quadruplex DNA structures: Variations on a theme, *Biol. Chem. 382*, 621−628.
15. Wang, Y., and Patel, D. J. (1993) Solution structure of the human telomeric repeat d[$AG_3(T_2AG_3)_3$] G-tetraplex, *Structure 1*, 263−282.
16. Parkinson, G. N., Lee, M. P., and Neidle, S. (2002) Crystal structure of parallel quadruplexes from human telomeric DNA, *Nature 417*, 876−880.
17. Balagurumoorthy, P., and Brahmachari, S. K. (1994) Structure and stability of human telomeric sequence, *J. Biol. Chem. 269*, 21858−21869.
18. Ren, J., Qu, X., Trent, J. O., and Chaires, J. B. (2002) Tiny telomere DNA, *Nucleic Acids Res. 30*, 2307−2315.

19. Redon, S., Bombard, S., Elizondo-Riojas, M. A., and Chottard, J. C. (2003) Platinum cross-linking of adenines and guanines on the quadruplex structures of the $AG_3(T_2AG_3)_3$ and $(T_2AG_3)_4$ human telomere sequences in Na^+ and K^+ solutions, *Nucleic Acids Res. 31*, 1605−1613.
20. Lepre, C. A., and Lippard, S. J. (1990) Interaction of platinum antitumor compounds with DNA, *Nucleic Acids Mol. Biol. 4*, 9−38.
21. Ying, L., Green, J. J., Li, H., Klenerman, D., and Balasubramanian, S. (2003) Studies on the structure and dynamics of the human telomeric G quadruplex by single-molecule fluorescence resonance energy transfer, *Proc. Natl. Acad. Sci. U.S.A. 100*, 14629−14634.
22. Farrell, N., Qu, Y., Bierbach, U., Valsecchi, M., and Menta, E. (1999) Structure−Activity Relationships within Di- and Trinuclear Platinum Phase-I Clinical Anticancer Agents, in *Cisplatin: Chemistry and biochemistry of a leading anticancer drug* (Lippert, B., Ed.) pp 479−496, Wiley-VCH, Zurich.
23. Burstyn, J. N., Heiger-Bernays, W. J., Cohen, S. M., and Lippard, S. J. (2000) Formation of cis-diamminedichloroplatinum(II) 1,2-intrastrand cross-links on DNA is flanking-sequence independent, *Nucleic Acids Res. 28*, 4237−4243.
24. Kasparkova, J., Farrell, N., and Brabec, V. (2000) Sequence specificity, conformation, and recognition by HMG1 protein major DNA interstrand cross-links of antitumor dinuclear platinum complexes, *J. Biol. Chem. 275*, 15789−15798.
25. Farrell, N., Qu, Y., Feng, L., and Van Houten, B. (1990) Comparison of Chemical Reactivity, Cytotoxicity, Interstrand Cross-Linking and DNA Sequence Specificity of Bis(platinium) Complexes Containing Monodentate or Bidentate Coordination Spheres with Their Monomeric Analogues, *Biochemistry 29*, 9522−9531.
26. Reeder, F., Kozelka, J., and Chottard, J. C. (1996) Triammineplatinum(II) Coordinated to a Guanine Does Not Prevent Platination of an Adjacent Guanine in Single-Stranded Oligonucleotides, *Inorg. Chem. 35*, 1413−1415.
27. Kasparkova, J., Mellish, K. J., Qu, Y., Brabec, V., and Farrell, N. (1996) Site-specific d(GpG) intrastrand cross-links formed by dinuclear platinum complexes. Bending and NMR studies, *Biochemistry 35*, 16705−16713.
28. Zou, Y., Van Houten, B., and Farrell, N. (1994) Sequence specificity of DNA-DNA interstrand cross-link formation by cisplatin and dinuclear platinum complexes, *Biochemistry 33*, 5404−5410.
29. Redon, S., Bombard, S., Elizondo-Riojas, M. A., and Chottard, J. C. (2001) Platination of the $(T_2G_4)_4$ telomeric sequence: A structural and cross-linking study, *Biochemistry 40*, 8463−8470.
30. Case, D. A., Pearlman, D. A., Caldwell, J. M., Cheatman, T. E., III, Wang, J., Ross, W. S., Simmerling, C. L., Darden, T. A., Merz, K. M., Stanton, R. V., Cheng, A. L., Vincent, J. J., Crowley, M., Tsui, V., Gohlke, H., Radmer, R. J., Duan, Y., Pitera, J., Massova, I., Seibel, G. L., Singh, U. C., Weiner, P. K., and Kollman, P. A. (2002) *AMBER 7.0*, University of California, San Francisco.
31. Tsui, V., and Case, D. A. (2000) Molecular dynamics simulations of nucleic acids with a generalized Born solvation model, *J. Am. Chem. Soc. 122*, 2489−2498.
32. Cheatham, T. E., Cieplack, I. P., and Kollman, P. A. (1999) A modifed version of the Cornell et al. force field with improved sugar pucker phases and helical repeat, *J. Biomol. Struct. Dyn. 4*, 845−862.
33. Humphrey, W., Dalke, A., and Schulten, K. (1996) VMD: Visual Molecular Dynamics, *J. Mol. Graphics 14.1*, 33−38.
34. Montjardet-Bas, V., Elizondo-Riojas, M. A., Chottard, J. C., and Kozelka, J. (2002) A combined effect of molecular electrostatic potential and N7 accessibility explains sequence-dependent binding of *cis*-$[Pt(NH_3)_2(H_2O)_2]^{2+}$, *Angew. Chem., Int. Ed. 41*, 2998−3001.
35. Frisch, M. J., Trucks, G. W., Schlegel, H. B., Scuseria, G. E., Robb, M. A., Cheeseman, J. R., Montgomery, J. J. A., Vreven, T., Kudin, K. N., Burant, J. C., Millam, J. M., Iyengar, S. S., Tomasi, J., Barone, V., Mennucci, B., Cossi, M., Scalmani, G., Rega, N., Petersson, G. A., Nakatsuji, H., Hada, M., Ehara, M., Toyota, K., Fukuda, R., Hasegawa, J., Ishida, M., Nakajima, T., Honda, Y., Kitao, O., Nakai, H., Klene, M., Li, X., Knox, J. E., Hratchian, H. P., Cross, J. B., Adamo, C., Jaramillo, J., Gomperts, R., Stratmann, R. E., Yazyev, O., Austin, A. J., Cammi, R., Pomelli, C., Ochterski, J. W., Ayala, P. Y., Morokuma, K., Voth, G. A., Salvador, P., Dannenberg, J. J., Zakrzewski, V. G., Dapprich, S., Daniels, A. D., Strain, M. C., Farkas, O., Malick, D. K., Rabuck, A. D., Raghavachari, K., Foresman, J. B., Ortiz, J. V., Cui, Q., Baboul, A. G., Clifford, S., Cioslowski, J., Stefanov, B. B., Liu, G., Liashenko, A., Piskorz, P., Komaromi, I., Martin, R. L., Fox, D. J., Keith, T., Al-Laham, M. A., Peng, C. Y., Nanayakkara, A., Challacombe, M., Gill, P. M. W., Johnson, B., Chen, W., Wong, M. W., Gonzalez, C., and Pople, J. A. (2003) *Gaussian 03*, Gaussian, Inc., Pittsburgh, PA.
36. Besler, B. H., Merz, K. M. J., and Kollman, P. A. (1990) Atomic charges derived from semiempirical methods, *J. Comput. Chem. 11*, 431−439.
37. Ellis, L. T., and Hambley, T. W. (1994) Dichloro(ethylenediamine)platinum(II), *Acta Crystallogr. C50*, 1888−1889.
38. Arvanitis, G. M., Gibson, D., Emge, T. J., and Berman, H. M. (1994) Platinum(II) triamine complexes: cis-$[PtCl(NH_3)_2$-$(C_{10}H_{13}N_5O_5)]NO_3 \cdot 2H_2O$ and $[PtCl(C_2H_8N_2)(C_4H_6N_2)]NO_3$, *Acta Crystallogr. C50*, 1217−1220.
39. Michalska, D., and Wysokinski, R. (2004) Molecular Structure and Bonding in Platinum-Picoline Anticancer Complex: Density Functional Study, *Collect. Czech. Chem. Commun. 69*, 63−71.
40. Herman, F., Kozelka, J., Stoven, V., Guittet, E., Girault, J. P., Huynh-Dinh, T., Igolen, J., Lallemand, J. Y., and Chottard, J. C. (1990) A d(GpG)-platinated decanucleotide duplex is kinked: An extended NMR and molecular mechanics study, *Eur. J. Biochem. 194*, 119−133.
41. Elizondo-Riojas, M.-A., Gonnet, F., Auge-Barrere-Mazouat, P., Allain, F., Berges, J., Attias, R., Chottard, J. C., and Kozelka, J. (1997) Molecular modeling of platinum complexes with oligonucleotides: Methodological lessons and structural insights, in *Molecular Modeling and Dynamics of Bioinorganic Systems* (Banci, L., and Comba, P., Eds.) pp 131−160, Kluwer Academic Publishers, Dordrecht, The Netherlands.
42. Chval, Z., and Síp, M. (1998) Force field for platinum binding to adenine and guanine taking into account flexibility of nucleic acids bases, *J. Phys. Chem. 102*, 1659−1661.
43. Phan, A. T., and Mergny, J. L. (2002) Human telomeric DNA: G-Quadruplex, i-motif and Watson−Crick double helix, *Nucleic Acids Res. 30*, 4618−4625.
44. Henderson, E. R., Moore, M., and Malcolm, B. A. (1990) Telomere G-strand structure and function analyzed by chemical protection, base analogue substitution, and utilization by telomerase in vitro, *Biochemistry 29*, 732−737.
45. Stefl, R., Spackova, N., Berger, I., Koca, J., and Sponer, J. (2001) Molecular dynamics of DNA quadruplex molecules containing inosine, 6-thioguanine and 6-thiopurine, *Biophys. J. 80*, 455−468.
46. Bombard, S., Favre, A., and Kozelka, J. (1998) Very short oligonucleotides migrate on 20% polyacrylamide gels with an apparent friction coefficient proportional to molecular mass, *Anal. Biochem. 263*, 123−125.
47. Escaffre, M., Favre, A., Chottard, J. C., and Bombard, S. (2002) Determination of platinated purines in oligoribonucleotides by limited digestion with ribonucleases T1 and U2, *Anal. Biochem. 310*, 42−49.
48. Seenisamy, J., Rezler, E. M., Powell, T. J., Tye, D., Gokhale, V., Joshi, C. S., Siddiqui-Jain, A., and Hurley, L. H. (2004) The dynamic character of the G-quadruplex element in the c-MYC promoter and modification by TMPyP4, *J. Am. Chem. Soc. 126*, 8702−8709.
49. He, Y. J., Neumann, R. D., and Panyutin, I. G. (2004) Intramolecular quadruplex conformation of human telomeric DNA assessed with I-125-radioprobing, *Nucleic Acids Res. 32*, 5359−5367.
50. Phan, A. T., and Patel, D. J. (2003) Two-repeat human telomeric d(TAGGGTTAGGGT) sequence forms interconverting parallel and antiparallel G-quadruplexes in solution: Distinct topologies, thermodynamic properties, and folding/unfolding kinetics, *J. Am. Chem. Soc. 125*, 15021−15027.
51. Miyoshi, D., Nakao, A., Toda, T., and Sugimoto, N. (2001) Effect of divalent cations on antiparallel G-quartet structure of $d(G_4T_4G_4)$, *FEBS Lett. 496*, 128−133.
52. Miyoshi, D., Nakao, A., and Sugimoto, N. (2003) Structural transition from antiparallel to parallel G-quadruplex of $d(G_4T_4G_4)$ induced by Ca^{2+}, *Nucleic Acids Res. 31*, 1156−1163.
53. Hardin, C. C., Corregan, M. J., Lieberman, D. V., and Brown, B. A., II (1997) Allosteric interactions between DNA strands and monovalent cations in DNA quadruplex assembly: Thermodynamic evidence for three linked association pathways, *Biochemistry 36*, 15428−15450.
54. Mergny, J. L., Phan, A. T., and Lacroix, L. (1998) Following G-quartet formation by UV-spectroscopy, *FEBS Lett. 435*, 74−78.

55. Hud, N. V., Smith, F. W., Anet, F. A., and Feigon, J. (1996) The selectivity for K^+ versus Na^+ in DNA quadruplexes is dominated by relative free energies of hydration: A thermodynamic analysis by ^{1}H NMR, *Biochemistry 35*, 15383−15390.
56. Phan, A. T., Modi, Y. S., and Patel, D. J. (2004) Two-repeat *Tetrahymena* Telomeric d(TGGGGTTGGGGT) Sequence Interconverts Between Asymmetric Dimeric G-quadruplexes in Solution, *J. Mol. Biol. 338*, 93−102.
57. Gonnet, F., Kocher, F., Blais, J. C., Bolbach, G., and Tabet, J. C. (1996) Kinetic analysis of the reaction between d(TTGGCCAA) and $[Pt(NH_3)_3(H_2O)]^{2+}$ by enzymatic degradation of the products and ESI and MALDI mass spectrometries, *J. Mass Spectrom. 31*, 802−809.
58. Guittard, J., Pacifico, C., Blais, J. C., Bolbach, G., Chottard, J. C., and Spassky, A. (1995) Matrix-assisted laser desorption ionization time-of-flight mass spectrometry of DNA-Pt(II) complexes, *Mass Spectrom. 9*, 33−36.

BI050144W